JOURNAL OF NATURAL PRODUCTS

Article

pubs.acs.org/jnp

α-Glucosidase Inhibitors from *Salvia circinata*

Laura Flores-Bocanegra,[†] Martin González-Andrade,[‡] Robert Bye,[§] Edelmira Linares,[§] and Rachel Mata*[,†]

[†]Facultad de Química, [‡]Facultad de Medicina, and [§]Instituto de Biología, Universidad Nacional Autónoma de México, Cuidad de México 04510, México

Supporting Information

ABSTRACT: A dried infusion prepared from the aerial parts of *Salvia circinata* did not provoke acute toxicity in mice (LD_{50} > 5 g/kg). This infusion showed poor hypoglycemic and antihyperglycemic effects (100−570 mg/kg) when tested in normal and hyperglycemic mice using acute and oral glucose tolerance tests, respectively. However, this infusion possessed antihyperglycemic action in vivo during an oral sucrose tolerance test (31.6−316 mg/kg), suggesting the presence of α-glucosidase inhibitors in *S. circinata*. Fractionation of a nonpolar extract of the aerial parts of the plant yielded a new biflavone (**1**) and four new neoclerodane diterpenoid glucosides (**2**−**5**) along with the known compounds amarisolide (**6**), pedalitin (**7**), apigenin-7-*O*-β-D-glucoside (**8**), and the flavone 2-(3,4-dimethoxyphenyl)-5,6-dihydroxy-7-methoxy-4*H*-chromen-4-one (**9**). Compounds **1** and **6**−**9** were active against mammalian α-glucosidases; **6** and **7** were also active against a recombinant α-glucosidase from *Ruminococcus obeum* and reduced significantly the postprandial peak during an oral sucrose tolerance test in healthy mice, consistent with their α-glucosidase inhibitory activity. Molecular docking and dynamic studies revealed that compounds **6** and **7** might bind to α-glucosidases at the catalytic center of the enzyme.

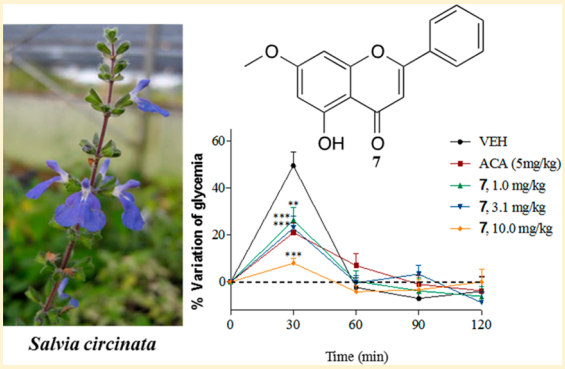

According to the International Diabetes Federation, in 2015 around 415 million people worldwide were suffering from type II diabetes mellitus (T2DM).[1] The high prevalence of this disease and its negative economic impact on global national health systems have triggered the search for new therapeutic alternatives. In particular, in middle- and low-income countries, diabetic patients require more economic and efficient treatments to ameliorate their impaired glycemic conditions. To assist with this problem, plants used in traditional medicine have proven to be valuable sources of phytotherapeutic preparations and chemical templates for the development of new antidiabetic drugs.[2] Thus, as part of our efforts to establish the efficacy of selected Mexican plants for treating diabetes and to discover new α-glucosidase inhibitors,[3−5] useful for the development of new antidiabetic therapies, reported herein is the investigation of *Salvia circinata* Cav. (Lamiaceae). Previous studies on other species of this genus, including *S. miltiorrhiza* Bunge,[6] *S. splendens* Sellow ex Schult.,[7] *S. hypoleuca* Benth.,[8] *S. fruticosa* Mill.,[9] *S. syriaca* L.,[10] *S. santolinifolia* Boiss.,[11] *S. moorcraftiana* Wall.,[12] *S. limbata* C.A. Mey.,[10] *S. atropatana* Bunge,[10] *S. nemorosa* L.,[10] and *S. multicaulis* Vahl.,[10] have revealed its potential as sources of hypoglycemic and α-glucosidase inhibitory agents. In most cases, the active ingredients have been flavonoids and other phenolic compounds such as salvianolic acids A and B, which ameliorated hyperglycemia and dyslipidemia in db/db mice through the AMPK pathway.[6] More recently, some clerodane diterpenoids from *S. chamaedryoides* Cav. were found to be active as α-glucosidase inhibitors in vitro against α-amylase from hog pancreas and α-glucosidase from *Saccharomyces cerevisiae*.[13]

S. circinata (syn. *Salvia amarissima* Ortega) is a perennial herb widely distributed in Mexico, mainly in the Central Mexican Valley, Oaxaca, and San Luís Potosí.[14] This species is used in folk medicine for treating ulcers, helminthiases, and diabetes.[15] Previous phytochemical studies led to the isolation of some clerodane diterpenoids such as amarisolide (**6**),[16,17] several *seco*-clerodane diterpenoids,[10] and the flavone pedalitin (**7**).[16] Some of the compounds obtained were cytotoxic against human cancer cell lines and had modulatory activity in a breast cancer cell line resistant to vinblastine.[17,18]

RESULTS AND DISCUSSION

Acute toxicity analysis in animals is the first step during the assessment of the efficacy of phytopreparations. The information obtained from an acute toxicity test is useful for choosing appropriate doses for pharmacological studies and providing preliminary identification of target organ toxicity. In this investigation, acute toxicity was studied in mice following the Lorke protocol,[19] which gives reproducible results using a minimum number of animals. Acute administration of a dried infusion prepared from the aerial parts of *S. circinata* did not provoke behavior alterations, macroscopic tissue injury, or

Received: February 21, 2017

DOI: 10.1021/acs.jnatprod.7b00155
J. Nat. Prod. XXXX, XXX, XXX−XXX

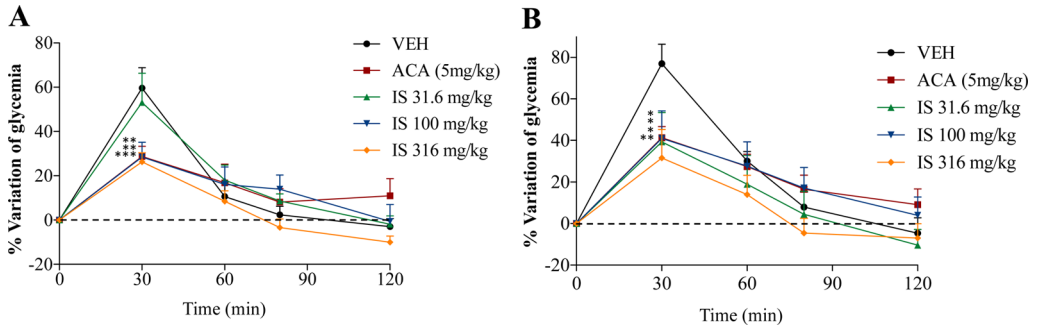

Figure 1. Antihyperglycemic action of the infusion (IS) from *S. circinata* (31.6−316 mg/kg, po) in normoglycemic (A) and NA-STZ (50/130 mg/kg, ip)-hyperglycemic mice (B) during an oral glucose tolerance test. VEH: vehicle; ACA: acarbose. Each point represents the mean ± SEM for 6 mice in each group. *$p < 0.05$, **$p < 0.01$, and ***$p < 0.001$ represent significantly different two-way ANOVA followed by Bonferroni's post hoc test for comparison with respect to vehicle control at the same time.

Chart 1

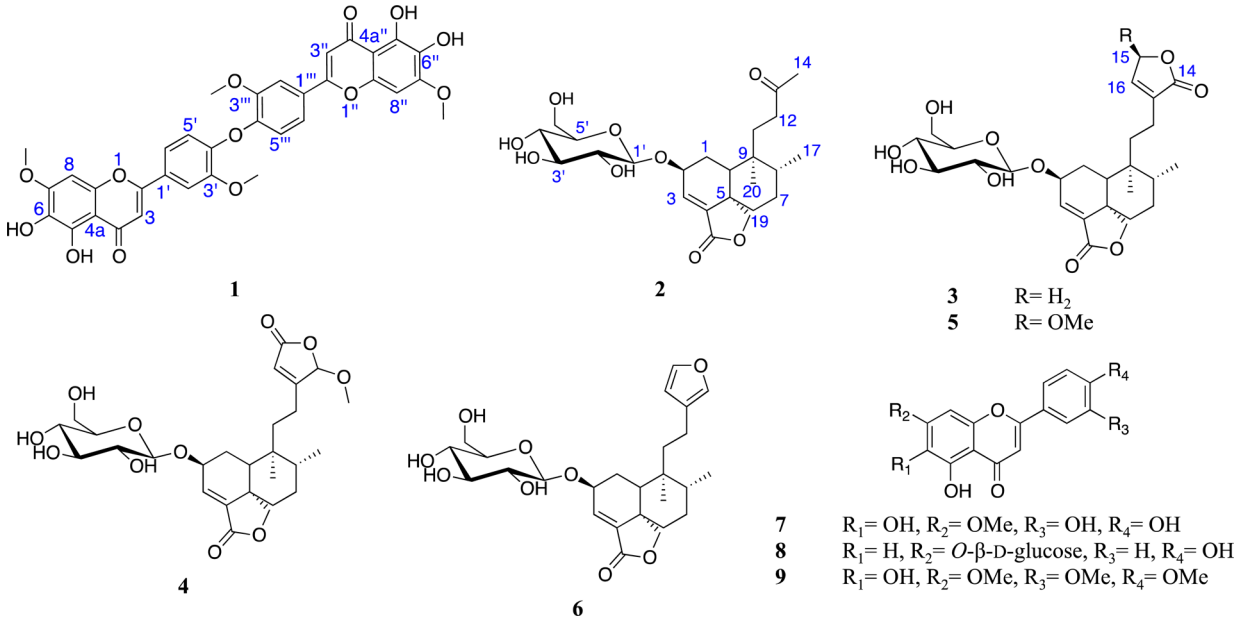

weight loss during a 14-day observation period, and the estimated LD_{50} was higher than 5 g/kg. Therefore, according to the Lorke criteria, the traditional preparation of *S. circinata* proved to be devoid of acute toxic effects for mice (Table S1, Supporting Information).

Next, the hypoglycemic potential of the *S. circinata* infusion was assessed in both normal and nicotinamide−streptozotocin (NA 50 mg/kg-STZ 130 mg/kg)-treated mice using half-log interval doses (100−570 mg/kg), chosen according to a standard protocol of allometric scaling.[20] The NA-STZ model is used for evaluating potential antidiabetic drugs since it portrays a similar biochemical blood profile and pathogenesis to T2DM in humans.[21] Oral administration of the infusion to normal and NA-STZ mice showed a moderate decrease of blood glucose level at the doses tested (Figure S1, Supporting Information). This effect was less than that produced by glibenclamide (GLI), an antidiabetic drug.

The antihyperglycemic effect of the *S. circinata* infusion was initially established throughout an oral glucose tolerance test (Figure S2, Supporting Information). In this, the infusion did not induce a significant drop in the postprandial peak after glucose challenge in normal and hyperglycemic mice (100−570 mg/kg). Finally, during an oral sucrose tolerance test (Figure 1), the infusion (31.6, 100, and 316 mg/kg) significantly reduced blood glucose when compared with a vehicle-treated group, with the effect observed comparable to that of acarbose, a commercially available drug used as positive control. The good activity observed during the oral sucrose tolerance test and the poor effect during the oral glucose tolerance test strongly suggested that the antihyperglycemic effect of the *S. circinata* infusion could be due to the presence of α-glucosidase inhibitors, which may be able to prevent postprandial hypersecretion of insulin and reactive hypoglycemia.[22]

In order to isolate the active principles, a nonpolar extract from the aerial parts of *S. circinata* was prepared. Extensive chromatography of this extract yielded new compounds **1**−**5**, along with the known substances **6**,[16] **7**,[16] **8**,[23] and **9**,[24] which were identified by comparison with physical and spectroscopic data previously reported.

Compound **1** was isolated as a yellow, amorphous powder. Its molecular formula, $C_{34}H_{26}O_{13}$, was calculated from the HRESIMS. The IR spectrum displayed characteristic signals for hydroxy and carbonyl groups (3252 and 1663 cm^{-1}, respectively). The chemical shifts of the paired signals in the NMR spectrum (Table 1, Figures S3 and S4, Supporting

DOI: 10.1021/acs.jnatprod.7b00155
J. Nat. Prod. XXXX, XXX, XXX−XXX

Table 1. ^{1}H (500 MHz) and ^{13}C (125 MHz) NMR Spectroscopic Data for Compound 1 in CD_3OD

position	δ_C	type	δ_H, multiplicity (J in Hz)
2	166.7,	C	
3	104.3,	CH	6.53, s
4	184.1,	C	
4a	107.0,	C	
5	147.6,	C	
6	156.2,	C	
7	131.8,	C	
8	92.4,	CH	6.71, s
8a	152.3,	C	
1′	131.9,	C	
2′	111.0,	CH	7.39, d (2.0)
3′	149.9,	C	
4′	152.5,	C	
5′	117.2,	CH	6.86, d (8.3)
6′	122.2,	CH	7.42, dd (8.4, 2.1)
2″	165.5,	C	
3″	104.5,	CH	6.49, s
4″	184.2,	C	
4a″	107.1,	C	
5″	147.6,	C	
6″	156.3,	C	
7″	131.9,	C	
8″	92.3,	CH	6.67, s
8a″	152.4,	C	
1‴	125.5,	C	
2‴	114.4,	CH	7.30, d 2.2
3‴	153.0,	C	
4‴	148.7,	C	
5‴	113.0,	CH	6.96, d (8.6)
6‴	120.5,	CH	7.38, dd (7.3, 2.1)
OCH_3-7	57.4,	CH_3	3.92, s
OCH_3-3′	57.0,	CH_3	3.90, s
OCH_3-7″	57.4,	CH_3	3.92, s
OCH_3-3‴	56.9,	CH_3	3.89, s

Information) were consistent with a biflavone-type dimeric flavonoid, with a C-4′ → C-4‴ interflavanoid ether linkage.[25,26] The ^{1}H NMR spectrum (Table 1 and Figure S3, Supporting Information) showed two ABX systems attributable to the protons of ring C of the two flavonoid moieties, which were then trisubstituted. Four singlets assigned to H-8 (δ_H 6.75), H-8″ (δ_H 6.69), H-3 (δ_H 6.58), and H-3″ (δ_H 6.55) were also observed; thus, rings A of both monomers were pentasubstituted. Finally, signals for four methoxy groups between δ_H 3.8 and 3.9 were detected. The cross-peaks observed for H-8 and H-8″ with the methoxy group signals in the NOESY spectrum indicated that two of the methoxy groups were at C-7 and C-7″. On the other hand, the NOESY correlations from H-2′ (δ_H 7.43) → OCH_3-3′ (δ_H 3.96) and H-2‴ (δ_H 7.33) → OCH_3-3‴ (δ_H 3.94) were used to locate the other two methoxy groups at C-3′ and C-3‴ (Figure S10, Supporting Information). The long-range HMBC correlations from H-5′ (δ_H 6.90) → C-1′ (δ_C 131.9) and C-3′ (δ_C 149.9) and H-5‴ (δ_H 7.03) → C-1‴ (δ_C 125.5) and C-3‴ (δ_C 153.0) as well as those for H-2′ (δ_H 7.39) and H-6′ (δ_H 7.42) → C-4′ (δ_C 152.5), and H-2‴ (δ_H 7.30) and H-6‴ (δ_H 7.38) → C-4‴ (δ_C 148.7), corroborated these assignments and established the interlinkage bond as C-4′−O−C-4‴. The ^{13}C NMR spectrum was fully assigned by means of the HSQC and HMBC experiments. On the basis of this evidence, compound **1** was characterized as 6,6″,3‴-trihydroxy-7,3′,7″-*O*-trimethylloniflavone.[25,26]

Compounds **2**−**5** were isolated as optically active, colorless, glassy solids. Their molecular formulas were deduced by HRESIMS as $C_{24}H_{36}O_9$, $C_{26}H_{36}O_{10}$, $C_{27}H_{38}O_{11}$, and $C_{27}H_{38}O_{11}$, respectively. The IR spectra of all compounds included bands in the range 3396 to 3385 and from 1763 to 1749 cm^{-1}, consistent with the presence of hydroxy and α,β-unsaturated-γ-lactone groups in the molecules. The IR spectrum of **2** showed also a band at 1705 cm^{-1} attributable to a carbonyl group. The NMR spectra of **2**−**5** (Tables 2 and 3, Figures S12−S39, Supporting Information) showed strong similarities to those of amarisolide (**6**), a *neo*-clerodane type of diterpenoid possessing a tricyclic skeleton with the six-membered rings *trans*-fused and an ethylfuran moiety. Also in common, clerodanes **2**−**6** exhibited signals for a β-glucopyranosyloxy moiety at C-2 and an α,β-unsaturated-γ-lactone at C-4/C-5. In order to demonstrated the D configuration of the β-glucopyranosyloxy moiety, compounds **2**−**6** were hydrolyzed with β-glucosidase; in all cases, the aqueous-soluble fraction showed identical optical rotation ($[\alpha]^{20}_D$ +30) and R_f (co-TLC) to those of an authentic sample of β-D-glucose. Comparison of the NMR data of **2**−**5** with **6** (Tables 2 and 3) revealed that the β-substituted furan ring in **6** was replaced by a methyl ketone group in **2**, an α,β-unsaturated-γ-lactone in **3**, and a five-membered ketolactol methyl ether in **4** and **5**. Assignments of the ^{1}H and ^{13}C NMR data of **2**−**5** (Tables 2 and 3) were supported by 2D NMR (^{1}H−^{1}H COSY, HSQC, and HMBC) experiments. The ^{13}C NMR chemical shifts observed in the spectra of compounds **4** and **5** for C-13 (**4**/**5** δ_C 170.0/137.9), C-14 (**4**/**5** δ_C 104.7/171.2), C-15 (**4**/**5** δ_C 171.0/102.5), and C-16 (**4**/**5** δ_C 117.2/143.0) revealed that the ethyl fragment [C-11 (**4**/**5** δ_C 27.6/34.7) and C-12 (**4**/**5** δ_C 33.9/17.7)] is linked to the five-membered ketolactol methyl ether moiety at the β-[27,28] or α-[29,30] carbon to the carbonyl group, respectively. The HMBC correlations for H-12 and H-14 in **4** supported this assignment [H-12a (δ_H 1.56) → C-14 (δ_C 104.7); H-12b (δ_H 2.09) → C-14 (δ_C 104.7); and H-14 (δ_H 5.91) → C-12 (δ_C 33.9)]. Likewise, the HMBC correlations for H-12 and H-15 in **5** [H-12a (δ_H 2.33) → C-16 (δ_C 143.0); H-12b (δ_H 2.09) → C-16 (δ_C 143); and H-15 (δ_H 5.92) → C-13 (δ_C 137.9) and C-14 (δ_C 171.2)] reinforced the structural assignment made.

The NOESY interactions (Figure 2) observed in the spectra of **2**−**5** revealed that the relative configuration at the stereogenic centers of all clerodanes were identical to that of **6**. Thereafter, the electronic circular dichroism (ECD) spectra of **2**−**6** were simulated. The experimental and calculated ECD spectra (Figures 3 and S40, Supporting Information) were similar in all cases, indicating that the absolute configuration at the stereogenic centers C-2, C-5, C-8, C-9, and C-10 was *S*, *S*, *R*, *R*, and *R*, respectively, in **2**−**6**. All spectra showed negative Cotton effects at ∼208 and ∼250 nm due to the electronic transitions $\pi \rightarrow \pi^*$ and $n \rightarrow \pi^*$, respectively, of the α,β-unsaturated-γ-lactone. It is important to point out that the absolute configuration of **6** was unequivocally determined by X-ray analysis;[31] since the optical rotation of **6** isolated in this work was identical to that previously reported,[16,31] the strategy employed to establish the configuration at the streogenic centers at the tricyclic skeleton with the six-membered rings *trans*-fused of all diterpenes appears to be sound. In the case of compounds **4** and **5**, the ECD were calculated for the two possible epimers at C-14 or C-15, respectively. The results

DOI: 10.1021/acs.jnatprod.7b00155
J. Nat. Prod. XXXX, XXX, XXX−XXX

Table 2. ^{1}H (500 MHz) NMR Spectroscopic Data for Compounds 2−5 in DMSO-d_6

	δ, multiplicity (J, Hz)							
position	2		3		4		5	
1	1.76,	ddd (13.8, 12.0, 12.0)	1.80,	ddd (13.8, 12.0, 12.0)	1.76,	ddd (13.8, 12.0, 12.0)	1.81,	ddd (13.8, 12.0, 12.0)
	1.28,	m[a]	1.34,	m[a]	1.34,	m[a]	1.34,	m[a]
2	4.43,	m[a]	4.47,	m[a]	4.47,	m[a]	4.46,	m[a]
3	6.63,	d (6.4)	6.63,	d (6.4)	6.67,	d (6.3)	6.66,	d (6.3)
6	1.69,	m	1.72,	m	1.67,	m	1.71,	m
	1.18,	m	1.25,	m	1.25,	m	1.25,	m
7	1.52,	m	1.24,	m	1.54,	m	1.60,	m
8	1.53,	m	1.71,	m	1.67,	m	1.54,	m
10	2.12,	d (12.9)	2.27,	d (12.6)	2.25,	d (12.9)	2.24,	d (12.9)
11	1.44,	m	1.54,	m	1.54,	m	1.53,	m
			1.43,	m			1.44,	m
12	2.61,	m	2.37,	m	1.56,	m	2.33,	m
	2.32,	m	2.06,	m	2.09,	m	2.09,	m
14	2.05,	s			5.91,	d (0.8)		
15			4.79,	m			5.92,	brs
16			7.45,	t (1.6)	6.04,	t (0.7)	7.13,	brs
17	0.74,	d (6.6)	0.80,	d (6.6)	0.80,	d (6.4)	0.79,	d (6.5)
19	3.97,	d (8.1)	4.00,	d (8.3)	4.02,	d (8.3)	4.02,	d (8.3)
	4.53,	d (8.1)	4.38,	d (8.2)	4.38,	d (8.2)	4.39,	d (8.2)
20	0.51,	s	0.54,	s	0.56,	s	0.56,	s
1′	4.29,	d (7.7)	4.31,	d (7.7)	4.30,	d (7.7)	4.30,	d (7.7)
2′	2.94,	dd (8.0)	2.94,	dd (8.0)	2.97,	dd (8.0)	2.93,	dd (8.0)
3′	3.10,	dd (8.0)	3.11,	dd (8.0)	3.11,	dd (8.0)	3.10,	dd (8.0)
4′	2.96,	dd (8.0)	2.97,	dd (8.0)	2.98,	dd (8.0)	2.95,	dd (8.0)
5′	3.10,	m	3.11,	m	3.11,	m	3.10,	m
6′	3.65,	dd (11.3, 2.5)	3.60,	dd (11.0, 2.5)	3.67,	dd (11.6, 2.5)	3.64,	dd (11.6, 2.0)
	3.34,	m[a]	3.44,	m[a]	3.34,	m[a]	3.33,	m[a]
OCH_3					3.45,	s		
OCH_3							3.45,	s

[a]Signal overlapped.

revealed that the ECD calculated for the β-epimer at C-15 of **5** was identical to the experimental spectrum; thus, the absolute configuration at the chiral center C-15 in **5** was established as *S*. In the case of compound **4** the configuration at C-14 could not be established, since the calculated ECD spectra for the two epimers at C-14 did not match exactly with the experimental spectrum. On the basis of this evidence, compounds **2**−**5** were characterized as (2*S*,5*S*,8*R*,9*R*,10*R*)-2-(*O*-β-D-glucopyranosyl)-neocleroda-3-en-9-oxobutyl-18,19-olide (**2**), (2*S*,5*S*,8*R*,9*R*,10*R*)-2-(*O*-β-D-glucopyranosyl)neocleroda-3,13-diene-14,15;18,19-diolide (**3**), (2*S*,5*S*,8*R*,9*R*,10*R*)-2-(*O*-β-D-glucopyranosyl)neocleroda-14-methoxy-3,13-diene-15,14;18,19-diolide (**4**), and (2*S*,5*S*,8*R*,9*R*,10*R*,15*S*)-2-(*O*-β-D-glucopyranosyl)neocleroda-15-methoxy-3,13-diene-14,15;18,19-diolide (**5**), which were given the trivial names amarisolides B−E (**2**−**5**).

Compounds **1**−**9** were tested in vitro against mammalian α-glucosidase. The more active compounds were the flavonoids, and, in particular, compound **1** showed an IC_{50} value of 39 ± 0.06 μM, which was 2.5 times more active than acarbose (IC_{50} = 100 ± 0.3 μM), used as positive control. Flavonoids **7**−**9** exhibited IC_{50} values of 810 ± 39, 200 ± 12, and 1800 ± 140 μM, respectively. Regarding the diterpenoids, only compound **6** was active, with an IC_{50} value of 500 ± 32.3 μM. In the case of compounds **2**−**5**, the IC_{50} values were higher than 10 000 μM (Table S2, Supporting Information). The major compounds of the plant, **6** and **7**, and acarbose were also tested against a recombinant α-glucosidase with maltase-glucoamylase activity from *Ruminococcus obeum*, a bacterium found in the human intestine that is involved in carbohydrate metabolism.[32] This protein is a structural homologue to human intestinal *N*-maltase-glucoamylase (2QMJ.pdb, 85% coverage) with a highly conserved catalytic domain (Figures S41 and S42, Supporting Information). This enzyme is phylogenetically closer to human *N*-maltase-glucoamylase than those of rat small intestinal enzymes; therefore, it is possible to make better inferences regarding the potential in vivo effects in humans of any compound assayed with this enzyme. The maltase-glucoamylase enzyme from *R. obeum* shows substrate preference for α(1→6) over α(1→4) glycosidic linkages and produces glucose from isomaltose as well as maltose.[32] The results of the assays showed that **6**, **7**, and acarbose inhibited the activity of the pure enzyme with IC_{50} values of 400 ± 19.0, 60 ± 3.0, and 1030 ± 14.0 μM, respectively.

Compounds **6** and **7** were also evaluated in vivo in an oral sucrose tolerant test in healthy mice (Figure 4); acarbose was the positive control. As expected, oral administration of **6** and **7** reduced significantly the postprandial peak in a dose-dependent manner. In both cases, the effect was comparable to that of the positive control, thus revealing their antihyperglycemic potential. These results were consistent with the α-glucosidase inhibition activity demonstrated in vitro for these compounds.

In order to complete the inhibition studies, docking and molecular dynamics studies of the *R. obeum* α-glucosidase complexes were performed with acarbose, **6**, and **7** (Figures 5 and 6). According to the results obtained, the three products

DOI: 10.1021/acs.jnatprod.7b00155
J. Nat. Prod. XXXX, XXX, XXX−XXX

Table 3. ^{13}C (125 MHz) NMR Spectroscopic Data for Compounds 2−5 in DMSO-d_6

	δ, type							
position	2		3		4		5	
1	25.7,	CH_2	25.7,	CH_2	26.8,	CH_2	25.7,	CH_2
2	69.2,	CH	69.0,	CH	69.1,	CH	69.2,	CH
3	130.6,	CH	130.7	CH	131.0,	CH	130.8,	CH
4	142.8,	C	142.6,	C	143.2,	C	142.6,	C
5	45.1,	C	45.1,	C	45.6,	C	45.1,	C
6	33.6,	CH_2	33.3,	CH_2	33.7,	CH_2	33.3,	CH_2
7	27.2,	CH_2	27.2,	CH_2	26.2,	CH_2	27.2,	CH_2
8	35.8,	CH	35.8,	CH	35.9,	CH	35.7,	CH
9	36.8,	C	37.4,	C	37.7,	C	37.4,	C
10	39.3,	CH	39.2,	CH	39.5,	CH	39.2,	CH
11	30.3,	CH_2	34.9,	CH_2	27.6,	CH_2	34.7,	CH_2
12	36.0,	CH_2	17.8,	CH_2	33.9,	CH_2	17.7,	CH_2
13	208.7,	C	132.8,	C	170.0,	C	137.9,	C
14	30.0,	CH_3	174.2,	C	104.7,	CH	171.2,	C
15			70.4,	CH	171.0,	C	102.5,	CH
16			146.4,	CH	117.2,	CH	143.0,	CH
17	15.5,	CH_3	15.4,	CH_3	15.9,	CH_3	15.5,	CH_3
18	168.7,	C	168.8,	C	169.2,	C	168.8,	C
19	70.5,	CH_2	70.6,	CH_2	70.9,	CH_2	70.6,	CH_2
20	17.3,	CH_3	17.2,	CH_3	17.6,	CH_3	17.3,	CH_3
1′	101.9,	CH	101.9,	CH	102.0,	CH	102.8,	CH
2′	73.9,	CH	73.6,	CH	74.0,	CH	73.5,	CH
3′	76.8,	CH	76.7,	CH	77.2,	CH	76.7,	CH
4′	70.3,	CH	70.0,	CH	70.7,	CH	70.8,	CH
5′	77.0,	CH	76.9,	CH	77.4,	CH	77.0,	CH
6′	61.2,	CH_2	61.1,	CH_2	61.8,	CH_2	61.2,	CH_2
OCH_3					56.5,	OCH_3		
OCH_3							56.1,	OCH_3

bind to the catalytic site of the enzyme. On the other hand, the molecular dynamics studies (Figure 6) indicated that the total energy of the complexes remained stable throughout the analysis, revealing that the binding of the compounds was stable. The study was conducted for 20 ns considering that the system was stable during this period of time (Figure S44, Supporting Information). The most stable complex was compound 7 since the calculated ΔG was -31.26 ± 2.9, while the ΔG values for acarbose and **6** were -23.12 ± 4.6 and -20.03 ± 3.4, respectively. These results are in agreement with the inhibition data (IC_{50}) obtained experimentally. Animated images of the trajectories of molecular dynamics may be found in the Supporting Information (Figure S43).

In summary, the aerial parts of *S. circinata* possess an antihyperglycemic action in vivo in an oral sucrose tolerance test, supporting the medicinal use of *S. circinata* for treating diabetes in Mexican folk medicine. This plant produces several flavonoid and clerodane diterpene glycoside constituents with α-glucosidase inhibitory effects in vitro, and this target seems to be involved in their in vivo antihyperglycemic action. The maltase-glucoamylase enzyme from *R. obeum* demonstrated to be a good tool to assess α-glucosidase inhibitory activity in vitro. Molecular docking and dynamic studies revealed that compounds **6** and 7 might bind to α-glucosidase at the catalytic center of the enzyme. As hypothesized by Bisio et al.,[13] the enzymatic inhibitory capacity of species of *Salvia* is due not only to their content of phenolic compounds but also of other secondary metabolites such as the clerodane-type diterpenes, which are characteristic metabolites of this genus. To our knowledge, this is the first report of the in vivo action of a *neo*-clerodane diterpenoid against α-glucosidase and of the occurrence of biflavones in the genus *Salvia*.

EXPERIMENTAL SECTION

General Experimental Procedures. Melting points were determined on a Fisher-Johns apparatus and are uncorrected. IR, UV, and ECD spectra were recorded using a PerkinElmer 400 FT-IR, a Shimadzu U160, and a JASCO J720 instrument, respectively. Optical rotations were recorded at the sodium D-line wavelength using a PerkinElmer model 343 polarimeter at 20 °C. 1D and 2D NMR spectra were recorded in CD_3OD or DMSO-d_6 solution on a Bruker Avance III HD spectrometer at either 500 MHz (^1H) or 125 MHz (^{13}C) or a Varian VNRMS at 400 MHz (^1H) or 100 MHz (^{13}C), using tetramethylsilane as an internal standard. HRESIMS were obtained using a Thermo LTQ Orbitrap XL mass spectrometer. Preparative HPLC was carried out with a Waters instrument (Milford, MA, USA) equipped with a 2535 pump and a 2998 photodiode array detector, using an XBridge C_{18} packed column (21.1 × 250 mm) and different gradient systems of MeCN and 0.1% aqueous formic acid, at a flow rate of 17.0 mL/min. Control of equipment, data acquisition and processing, and management of chromatographic information were performed by the Empower 3 software package (Waters). Column chromatography (CC) was carried out on Sephadex LH-20 (GE Healthcare, Little Chalfont, Buckinghamshire, UK) and/or silica gel 60 (0.063−0.200). Each Sephadex LH-20 column was 60 cm long with 4 cm internal diameter. Thin-layer chromatographic analyses were performed on silica gel 60 F_{254} plates (Merck, Kenilworth, NJ, USA), and visualization of the plates was carried out using a $Ce_2(SO_4)_3$ (10%) solution in H_2SO_4.

Plant Material. The aerial parts of *S. circinata* were collected in June 2014 in Huauchinango Puebla, Mexico. The plant was identified by authors R.B. and E.L. A voucher specimen (R. Bye and E. Linares

DOI: 10.1021/acs.jnatprod.7b00155
J. Nat. Prod. XXXX, XXX, XXX−XXX

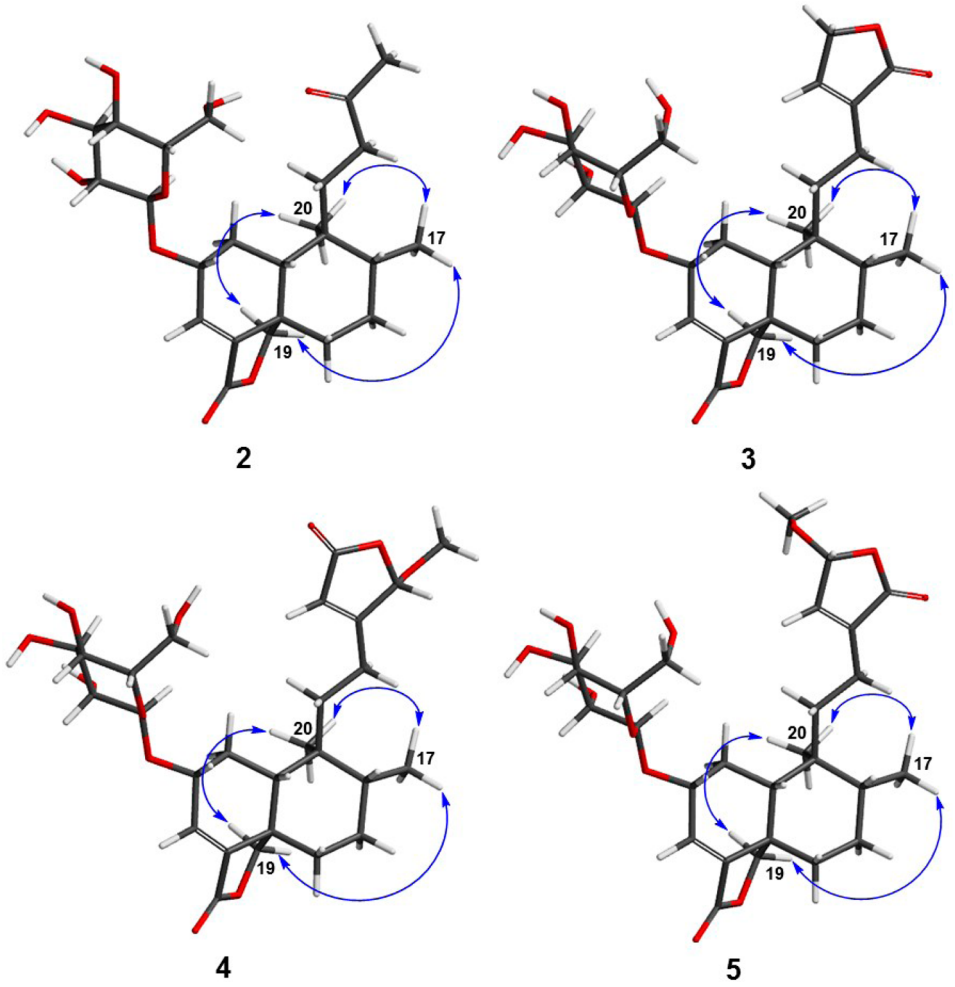

Figure 2. Key NOESY correlations of compounds **2**–**5**.

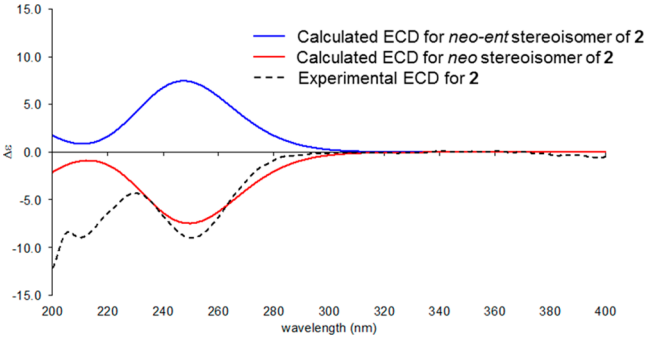

Figure 3. Comparison of theoretical and experimental ECD spectra of **2**.

37855) has been deposited at the National Herbarium (MEXU), UNAM, Mexico City.

Extraction and Isolation. Two hundred grams of dried and ground plant material was extracted with 5.5 L of boiling water for 20 min and was filtered and dried in vacuo to yield 19 g of aqueous extract. A nonpolar extract was prepared from 820 g of plant material by exhaustive maceration (8 days, three times) with 8 L of a solvent mixture of CH_2Cl_2–CH_3OH (1:1). Thereafter, the extract was filtered and dried in vacuo to yield 200 g of extract. A 150 g quantity of this extract was subjected to CC on silica gel (5000 g), eluting with hexane–EtAcO (100:0 → 0:100) and then with EtAcO–CH_3OH (100:0 → 80:20). This procedure yielded eight primary fractions (OE1–OE8). From fraction OE6, eluted with hexane–AcOEt (10:90), precipitated 3.87 g of **6** as a white solid, mp 206–208 °C. Fraction OE5 (6.3 g), eluted with hexane–AcOEt (40:60), was subjected to CC on Sephadex LH-20 eluting with CH_3OH to afford six secondary fractions (OE_51–OE_56). From fraction OE_56 (423.5 mg) precipitated **7** (368.0 mg) as a yellow solid, mp 300–302 °C. Fraction OE_53 (91.0 mg) was also subjected to CC on Sephadex LH-20 eluting with CH_3OH–acetone (1:1) to afford **1** (10.3 mg), mp 223–225 °C, and **9** (30.6 mg), mp 212–214 °C, both as yellow solids. Fraction OE6 (20 mg) was purified on a Sephadex LH-20 column (CH_3OH) to yield **8** (15.5 mg), mp 230–232 °C. Fraction OE7 (25 g) was separated on a silica gel column eluting with hexane–EtAcO (20:80 → 0:100) and then with EtAcO–CH_3OH (100:0 → 80:20) to afford four secondary fractions (OE_71–OE_74). Fractions OE_71 (53.0 mg) and OE_72 (75.3 mg) were purified by reversed-phase HPLC (XBridge C_{18}, 21.1 × 250 mm, 5 μm) using as mobile phase 30:70 MeCN–H_2O (acidified with 0.1% formic acid) and increasing linearly to 50% over 15 min at a flow rate of 17.0 mL/min. These processes yielded 25.0 mg of **3** (t_R 14.3 min) and 12.5 mg of **5** (t_R 17.0 min) from fraction OE_71 and 21.0 mg of **4** (t_R 16.2 min) and 17.0 mg of **2** (t_R 11.8 min) from fraction OE_72.

Compound ***1****:* yellow powder; mp 223–225 °C; UV (MeOH) λ_{max} (log ε) 271 (3.8), 330 (3.2) nm; IR (FTIR) ν_{max} 3252, 2925, 1663 cm^{-1}; ^1H and ^{13}C NMR in Table 1; HRESIMS *m*/*z* 643.1430 $[M + H]^+$ (calcd for $C_{34}H_{26}O_{13}$ $[M + H]^+$, 643.1452).

Compound ***2****:* glassy solid; $[\alpha]^{20}_D$ +54.73 (1 mg/mL, CH_3OH); UV (MeOH) λ_{max} (log ε) 206 (0.412); ECD (CH_3OH, c 0.1 mM, 0.1 cm); $\Delta\varepsilon$ −8.94 (210 nm), −8.98 (250 nm); IR (FTIR) ν_{max} 3378, 1763, 1705 cm^{-1}; ^1H and ^{13}C NMR in Table 2 and Table 3; HRESIMS *m*/*z* 469.2403 $[M + H]^+$ (calcd for $C_{24}H_{36}O_9$ $[M + H]^+$, 469.2438).

DOI: 10.1021/acs.jnatprod.7b00155
J. Nat. Prod. XXXX, XXX, XXX–XXX

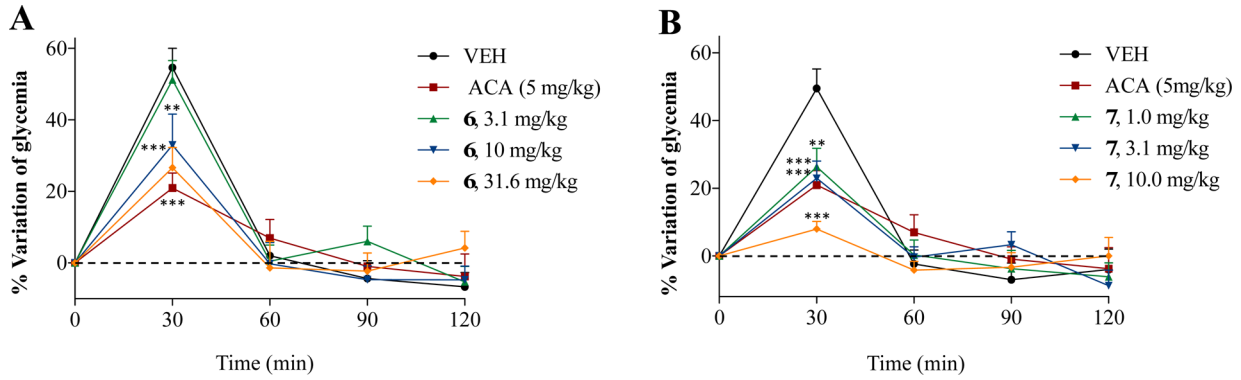

Figure 4. Antihyperglycemic action of **6** (A, 3.1−31.6 mg/kg, po) and **7** (B, 1.0−10.0 mg/kg, po) in normoglycemic mice during an OSTT. VEH: vehicle; ACA: acarbose. Each point represents the mean ± SEM for 6 mice in each group. $^{**}p < 0.01$ and $^{***}p < 0.001$ represent significantly different two-way ANOVA followed by Bonferroni's post hoc test for comparison with respect to vehicle control at the same time.

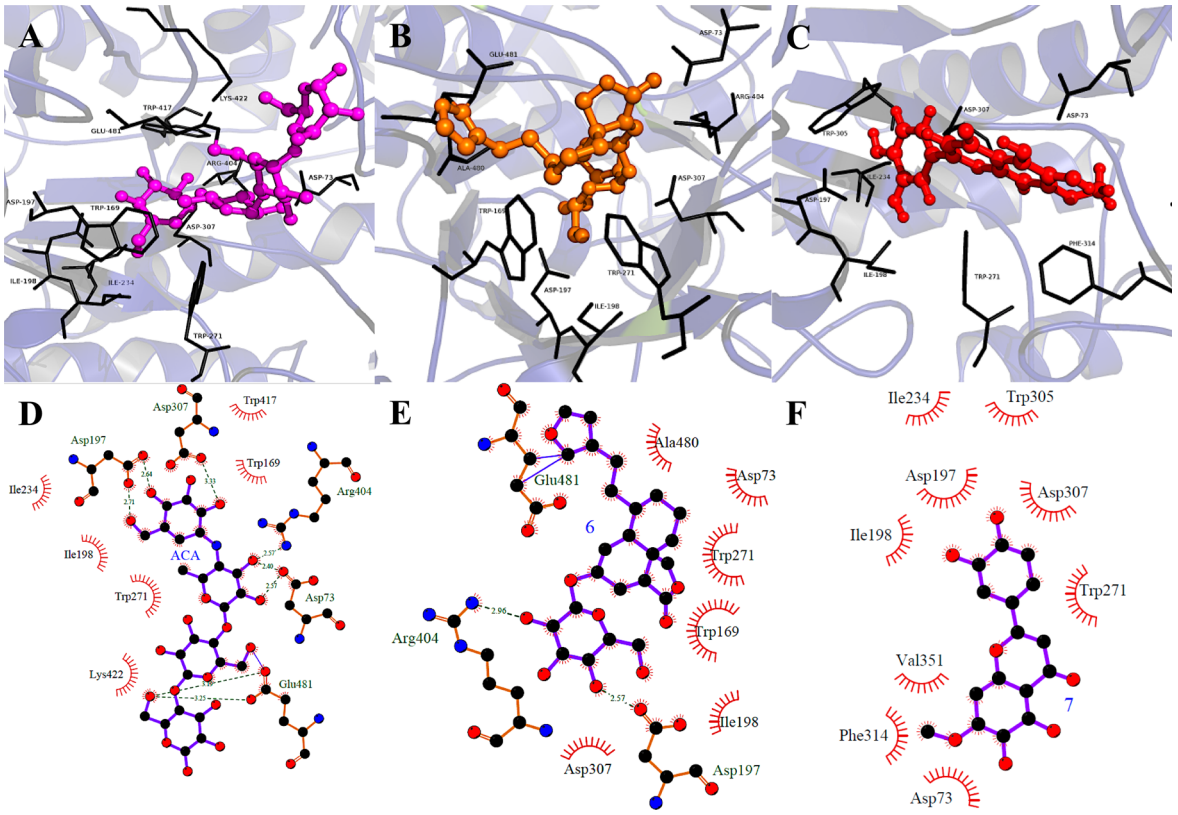

Figure 5. 3D Structural model of complexes of α-glucosidase with acarbose (A), **6** (B), and **7** (C). Binding sites and amino acid involved in the binding of acarbose (D), **6** (E), and **7** (F).

Compound ***3****:* glassy solid; $[\alpha]^{20}_{D}$ +43.05 (1 mg/mL, CH_3OH); UV (MeOH) λ_{max} (log ε) 207 (0.514); ECD (CH_3OH, *c* 0.1 mM, 0.1 cm); $\Delta\varepsilon$ −6.92 (208 nm), −7.29 (250 nm); IR (FTIR) ν_{max} at 3385, 1749 cm^{-1}; ^1H and ^{13}C NMR in Table 2 and Table 3; HRESIMS *m*/*z* 509.2352 $[M + H]^+$ (calcd for $C_{26}H_{36}O_{10}$ $[M + H]^+$, 509.2387).

Compound ***4****:* glassy solid; $[\alpha]^{20}_{D}$ +67.90 (1 mg/mL, CH_3OH); UV (MeOH) λ_{max} (log ε) 207 (0.631); ECD (CH_3OH, c 0.4 mM, 0.1 cm); $\Delta\varepsilon$ −16.4 (208 nm), −16.5 (250 nm); IR (FTIR) ν_{max} at 3396, 1754 cm^{-1}; ^1H and ^{13}C NMR in Table 2 and Table 3; HRESIMS *m*/*z* 539.2452 $[M + H]^+$ (calcd for $C_{27}H_{38}O_{11}$ $[M + H]^+$, 539.2492).

Compound ***5****:* glassy solid; $[\alpha]^{20}_{D}$ +59.21 (1 mg/mL, CH_3OH); ECD (CH_3OH, *c* 0.9 mM, 0.1 cm); $\Delta\varepsilon$ −15.92 (208 nm), −12.91 (251 nm); UV (MeOH) λ_{max} (log ε) 207 (0.614); IR (FTIR) ν_{max} at 3396, 1750 cm^{-1}; ^1H and ^{13}C NMR in Table 2 and Table 3; HRESIMS *m*/*z* 539.2455 $[M + H]^+$ (calcd for $C_{27}H_{38}O_{11}$ $[M + H]^+$, 539.2492).

Enzymatic Hydrolysis. Compounds **2**−**6** (5 mg each) were dissolved in phosphate buffer solution (5 mL, 100 mM at pH 7), and enzyme β-glucosidase (10 g, Sigma-Aldrich, St. Louis, MO, USA) was added to the solution and kept at 40 °C for 15 days, in each case. The reaction mixtures were extracted with $CHCl_3$, and the aqueous phases were compared directly with an authentic D-glucose sample by co-TLC and optical rotation.

Electronic Circular Dichroism Spectra. Minimum energy structures for the stereoisomers *neo*- and *ent*- of **2**−**6** were built with Spartan'10 software (Wavefunction Inc., Irvine, CA, USA). Conformational analysis was performed with the Monte Carlo search protocol as implemented in the same software under the MMFF94 molecular mechanics force field. The resulting conformers were minimized using the DFT method at the B3LYP/6-311G+(2d,p) level of theory. The time-dependent DFT (TDDFT) method at the B3LYP/6-31G+(d) level of theory was employed for ECD calculations using the same

DOI: 10.1021/acs.jnatprod.7b00155
J. Nat. Prod. XXXX, XXX, XXX−XXX

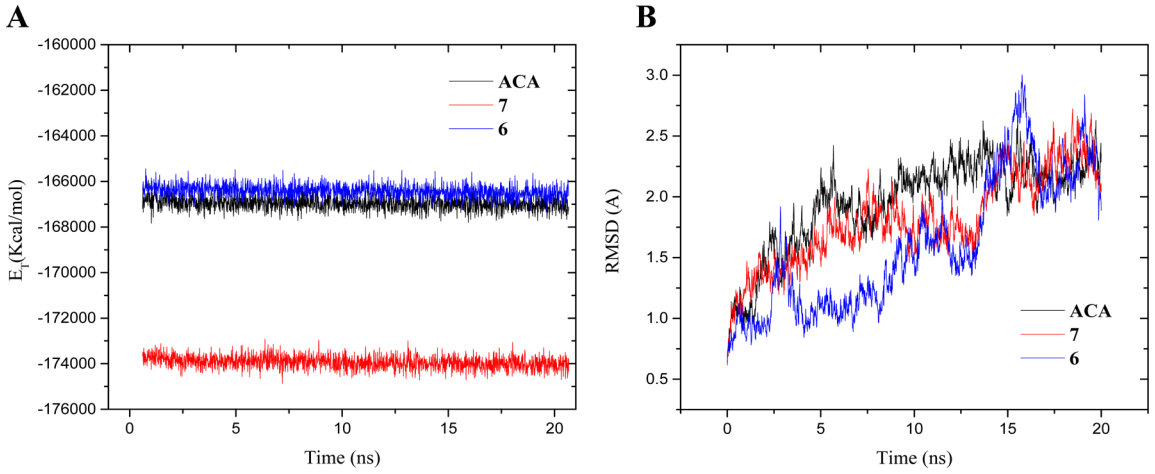

Figure 6. Molecular dynamics trajectory analysis. (A) Total energy of the system as a function of the time of **6**, **7**, and acarbose (ACA). (B) RMSD as a function of time.

DFT-minimized conformers. The self-consistent reaction field with a conductor-like continuum solvent model was used to perform the ECD calculations of the major conformers in MeOH. The calculated excitation energy (nm) and rotatory strength (R) in dipole velocity (Rvel) and dipole length (Rlen) forms were simulated into an ECD curve. All calculations were performed employing the Gaussian'09 program package (Gaussian Inc.).

α-Glucosidase Genetic Optimization, Cloning, Expression, and Purification. The α-glucosidase gene from *Ruminococcus obeum* ATCC 29174 was optimized (Figure S41, Supporting Information) for expression in *Escherichia coli* BL21(DE3), using the software OptimumGene from GenScript (Piscataway, NJ, USA). The optimized gene was cloned into the *pUC57* vector and subsequently subcloned into the expression vector *pET-12b* Novagen (EMD Chemicals, Darmstadt, Germany) using the restriction enzyme sites *Sal*I and *Bam*HI for their correct orientation. *E. coli BL21-DE3/pET12b* was grown in 500 mL of LB medium at 37 °C; the expression was induced by the addition of IPTG (0.5 mM). After 8 h, the cells were harvested by centrifugation (10 min, 4000*g*), suspended in 50 mM bis-TRIS propane at pH 8.0, and lysed by sonication with pulses of 5 min at an amplitude of 35% three times; cellular debris was removed by centrifugation (15 min × 15000*g*). The protein was identified by activity tests and gel electrophoresis.[32]

In Vitro Assay for α-Glucosidase Inhibitors. Acarbose, used as positive control, was dissolved in phosphate buffer solution (PBS, 100 mM, pH 7), and compounds **1**−**10** were dissolved in PBS or MeOH−PBS (1:1). The substrate used was *p*-nitrophenyl-α-D-glucopyranoside (20 mM in PBS; Sigma-Aldrich). The mammalian enzyme solution was prepared with 40 mg of rat intestinal acetone powder in 1 mL of PBS following the manufacturer's (Sigma-Aldrich) protocol. The *R. obeum* enzyme solution was used at a concentration of 5.2 mg/mL in bis-TRIS propane. Aliquots of 0−10 μL of compounds **1**−**9** and acarbose were incubated with 20 μL of enzyme solution in the case of the mammalian enzyme; in addition, compounds **6**, **7**, and acarbose were incubated with 5 μL of the enzyme solution of *R. obeum*; in both cases the incubation period was 10 min at 37 °C. After incubation, the substrate was added to each preparation (5 μL for mammalian and 10 μL for *R. obeum*), which were incubated for 30 min and 3 h more at 37 °C, respectively. Absorbances were determined in a Bio-Rad 680 microplate reader (Hercules, CA, USA) at 405 nm. The inhibitory activity expressed as IC_{50} was determined as previously described.[25,33]

Docking Protocol. Docking was conducted using the PDB X-ray structure of α-glucosidase from *R. obeum* (3N04.pdb); the structures of acarbose, **6**, and **7** were constructed using HyperChem 8 software and subsequently minimized using Gaussian 09, revision A.02 (Gaussian Inc., Wallingford, CT, USA).[34,35] Electrostatic grid maps, docking, and docking analyses were performed with AutoDockTools, AutoDock, and PyMOL softwares.[36]

Molecular Dynamics Simulation. The coordinates of the ligands, resulting from the docking study, were processed with an antechamber to generate suitable topologies for the LEaP module from AMBER 12.[37,38] Each structure and complex was subjected to the following protocol: Hydrogens were added using the LEaP module with the parm99 parameter set, Na^+ counterions were added to neutralize the system, and the structures were then solvated in an octahedral box of explicit TIP3P model water molecules, localizing the box limits at 12 Å from the protein surface.[39,40] MD simulations were performed. Frames were saved at 100 ps intervals for subsequent analysis. The analyses were conducted with *cpptraj*[41] on the trajectory time intervals where the convergence criteria were met. Binding free energies were calculated by molecular mechanics/Poisson−Boltzmann surface area.[42,43]

Experimental Animals. ICR male mice, aged between 3 and 4 weeks (25−30 g body weight), were obtained from Envigo Mexico RMS (CDMX). Animals were kept in an environmentally controlled room maintained at 22 ± 1 °C with an alternating 12 h light/dark natural cycle, with free access to standard rodent pellet diet (Teklad 2018S, Envigo) and water ad libitum until the beginning of each experiment. All animal experimental protocols were in conformity with the Mexican Official Norm for Animal Care and Handling (NOM-062-ZOO-1999) and the International Ethical Guidelines for the care and use of laboratory animals. The Ethical Committee for the Use of Animals in Pharmacological and Toxicological Testing, Facultad de Química-UNAM approved the protocols in March 2016: FQ/CICUAL/134/16 (Lorke assay) and FQ/CICUAL/132/16 (hypoglycemic and antihyperglycemic tests).

Acute Oral Toxicity in Mice of the Initial Infusion of *S. circinata*. The acute oral toxicity of the initial aqueous infusion of *S. circinata* was assessed and analyzed according to the Lorke method.[19] The dose schemes are provided in the Supporting Information.

Nicotinamide−Streptozotocin (NA-STZ)-Induced Experimental Hyperglycemia in Mice. Experimental hyperglycemia in mice was induced as described earlier,[4,21] using a single dose of NA (50 mg/kg) and STZ (130 mg/kg). One week later mice having blood glucose ≥ 200 mg/dL were considered hyperglycemic and selected for the study.

Collection of Blood Samples and Determination of Blood Glucose Levels. Blood samples were collected from the caudal vein, and the glucose levels (mg/dL) determined by the enzymatic glucose oxidase method as previously described.[4] The percentage variations of blood glucose levels were calculated following a standard protocol.[4]

Acute Hypoglycemic Assay. The hypoglycemic action of the dried plant initial infusion (100, 316, and 517 mg/kg) in normal and NA-STZ mice was performed following the procedures previously reported.[4] The percentage variation of glycemia was calculated as

DOI: 10.1021/acs.jnatprod.7b00155
J. Nat. Prod. XXXX, XXX, XXX−XXX

previously stated. Areas under the curve were calculated with the trapezoidal method.[4]

Oral Glucose Tolerance Test (OGTT). The antihyperglycemic action in an OGTT of the dried plant initial infusion (100, 316, and 517 mg/kg) in normal and NA-STZ mice was assayed following the methodology previously reported by our research group.[4]

Oral Sucrose Tolerance Test (OSTT). The antihyperglycemic action in an OSTT of the dried plant initial infusion (31.6, 100, and 316 mg/kg), **6** (3.1, 10, and 31.6 mg/kg), and **7** (1.0, 3.1, and 10 mg/kg) in normal and NA-STZ mice were assayed following the standard methodology reported elsewhere.[4]

Statistical Analysis. Data were expressed as means ± standard error. Statistical significance differences were ascertained by means of two-way ANOVA followed by Bonferroni's test for comparison with respect to vehicle control at the same time or ANOVA followed by Dunnett's test for comparison with respect to vehicle control. GraphPad Prism software (version 5.0, GraphPad Inc., La Jolla, CA, USA) was used for statistical analysis.

■ ASSOCIATED CONTENT

Supporting Information

The Supporting Information is available free of charge on the ACS Publications website at DOI: 10.1021/acs.jnatprod.7b00155.

Acute hypoglycemic action of an infusion from *S. cicrcinata* in normoglycemic and NA-STZ-hyperglycemic mice; antihyperglycemic action of an infusion from *S. cicrcinata* in normoglycemic and NA-STZ-hyperglycemic mice during an oral glucose tolerant test; one- and two-dimensional NMR spectra of compounds **1**−**5**; HRESIMS of **1**−**5**; alignment of the synthetic gene ATCC29174 after optimization; animated images of the trajectories of molecular dynamics of complexes acarbose-α-glucosidase, **6**-α-glucosidase, and **7**-α-glucosidase; molecular dynamics process; potential acute toxicity of an infusion from *S. cicrcinata* in mice assessed by the Lorke method; and inhibition of mammal α-glucosidases of compounds **2**−**5** (PDF)

■ AUTHOR INFORMATION

Corresponding Author

*Phone: +52-555-622-5289. E-mail: rachel@unam.mx.

ORCID

Rachel Mata: 0000-0002-2861-2768

Notes

The authors declare no competing financial interest.

■ ACKNOWLEDGMENTS

This work was supported by grants from CONACyT 219765, DGAPA IN217516 and IA 204116, and PAIP-UNAM 5000-9140. We thank R. del Carmen, I. Rivero-Cruz, M. Gutiérrez, A. Peréz-Vásquez, M. I. Velásquez López, and R. I. del Villar for their valuable technical assistance. We are indebted to Dirección General de Cómputo y de Tecnologías de Información y Comunicación (DGTIC), UNAM, for the resources to carry out computational calculations through the Miztli supercomputing system. L. F.-B. acknowledges CONACyT for a fellowship to pursue graduate studies.

■ REFERENCES

(1) *IDF Diabetes Atlas*, 7th ed.; International Diabetes Federation. Available at http://www.diabetesatlas.org (accessed January 10, 2017).

(2) Hung, H.; Quian, K.; Morris-Natschke, S.; Hsu, C.; Lee, K.-H. *Nat. Prod. Rep.* **2012**, *29*, 580−606.

(3) Anaya-Eugenio, G.; Rivero-Cruz, I.; Rivera-Chávez, J.; Mata, R. *J. Ethnopharmacol.* **2014**, *155*, 416−425.

(4) Ovalle-Magallanes, B.; Medina-Campos, O. N.; Pedraza-Chaverri, J.; Mata, R. *Phytochemistry* **2014**, *110*, 111−119.

(5) Martínez, A. L.; Madariaga-Mazón, A.; Rivero-Cruz, I.; Bye, R.; Mata, R. *Planta Med.* **2017**, *83*, 534.

(6) Huang, M.-Q.; Zhou, C.-J.; Zhang, Y.-P.; Zhang, X.-Q.; Xu, W.; Lin, J.; Wang, P.-J.; Ahmed Hamed, G. *Cell. Physiol. Biochem.* **2016**, *40*, 933−943.

(7) Fatma Abd-Elkader, M.; Mohamed-Soubhi, M.; Siham Mustafa, E.-S.; Wafaa Mostafa, E. K. *J. Pharm. Pharmacol.* **2012**, *64*, 1678−1687.

(8) Estakhr, J.; Javdan, N. *Pharmacologyonline* **2011**, *3*, 354−360.

(9) Perfumi, M.; Arnold, N.; Tacconi, R. *J. Ethnopharmacol.* **1991**, *34*, 135−40.

(10) Eskandani, M.; Bahadori, M. B.; Zengin, G.; Dinparast, L.; Bahadori, S. *Curr. Bioact. Compd.* **2016**, *12*, 34−38.

(11) Bahadori, M. B.; Valizadeh, H.; Asghari, B.; Dinparast, L.; Bahadori, S.; Farimani, M. M. *Curr. Bioact. Compd.* **2016**, *12*, 297−305.

(12) Khan, T.; Zahid, M.; Asim, M.; Shahzad, u.-H.; Iqbal, Z.; Choudhary, M. I.; Ahmad, V. U. *Phytomedicine* **2002**, *9*, 749−752.

(13) Bisio, A.; De Mieri, M.; Milella, L.; Schito, A. M.; Parricchi, A.; Russo, D.; Alfei, S.; Lapillo, M.; Tuccinardi, T.; Hamburger, M.; De Tommasi, N. *J. Nat. Prod.* **2017**, *80*, 503.

(14) Calderón, G.; Rzedowski, J. *INECOL* **2005**, *135*, 1−163.

(15) López, F. C.; Sánchez, D. M. G.; Arrieta, D.; Román, G. J. *Ciencia y Tecnología* **2010**, *9*, 67−76.

(16) Maldonado, E.; Cárdenas, J.; Bojórquez, H.; Escamilla, E. M.; Ortega, A. *Phytochemistry* **1996**, *42*, 1105−1108.

(17) Bautista, E.; Fragoso-Serrano, M.; Ortiz-Pastrana, N.; Toscano, R. A.; Ortega, A. *Fitoterapia* **2016**, *114*, 1−6.

(18) Bautista, E.; Fragoso-Serrano, M.; Toscano, R. A.; García-Peña, M. R.; Ortega, A. *Org. Lett.* **2015**, *17*, 3280−3282.

(19) Lorke, D. *Arch. Toxicol.* **1983**, *54*, 275−287.

(20) Wojcikowski, K.; Gobe, G. *Phytother. Res.* **2014**, *28*, 22−27.

(21) Ghosh, S.; Rangan, L. *Appl. Biochem. Biotechnol.* **2015**, *175*, 1477−1489.

(22) Suzuki, K.; Katsura, D.; Sagara, M.; Aoki, C.; Nishida, M.; Aso, Y. *Intern. Med.* **2016**, *55*, 949−953.

(23) Švehlíková, V.; Bennett, R.; Mellon, F. A.; Needs, P. W.; Piacente, S.; Kroon, P. A.; Bao, Y. *Phytochemistry* **2004**, *65*, 2323−2332.

(24) Bhardwaj, D. K.; Gupta, A. K.; Jain, A.; Shrawat, V. K. *Indian J. Chem.* **1988**, *27B*, 261−263.

(25) Oliveira, M. C. C.; Carvalho, M. G.; Silva, J. C.; Werle, A. A. *J. Braz. Chem. Soc.* **2002**, *13*, 119−123.

(26) Kumar, N.; Singh, B.; Bhandari, P.; Gupta, A. P.; Sanjay, K.; Vijay, K. K. *Phytochemistry* **2005**, *66*, 2740−2711.

(27) Du, K.; De Mieri, M.; Neugurger, M.; Zietsman, C. P.; Marston, A.; van Vuuren, S. F.; Ferreira, D.; Hamburger, M.; van der Westhuizen, J. *J. Nat. Prod.* **2015**, *78*, 2494−2504.

(28) Wu, T. H.; Cheng, Y. Y.; Liou, J. R.; Way, T. D.; Chen, C. J.; Kuo, S. C.; El-Shazly, M.; Chang, F. R.; Wu, Y. H.; Liaw, C. C. *RSC Adv.* **2014**, *4*, 23707−23712.

(29) Omosa, L. K.; Midiwo, J. O.; Derese, S.; Yenesew, A.; Peter, M. G.; Heydenreich, M. *Phytochem. Lett.* **2010**, *3*, 217−220.

(30) Omosa, L. K.; Amugune, B.; Ndunda, B.; Milugo, T. K.; Heydenreich, M.; Yenesew, A.; Midiwo, J. O. *S. Afr. J. Bot.* **2014**, *91*, 58−62.

(31) Toscano, A. R.; Maldonado, A.; Ortega, A.; Cárdenas, J. *Acta Crystallogr., Sect. C: Cryst. Struct. Commun.* **2001**, *C57*, 846−847.

(32) Tan, K.; Tesar, C.; Wilton, R.; Keigher, L.; Badnigg, G.; Joachimiak, A. *FASEB J.* **2010**, *24*, 3939−3949.

(33) Copeland, R. A. *Enzymes: A Practical Introduction to Structure, Mechanism, and Data Analysis*, 2nd ed.; Wiley-VCH: Weinheim, Germany, 2000; p 416.

DOI: 10.1021/acs.jnatprod.7b00155
J. Nat. Prod. XXXX, XXX, XXX−XXX

(34) Morris, G. M.; Goodsell, D. S.; Halliday, R. S.; Huey, R.; Hart, W. E.; Belew, R. K.; Olson, A. J. *J. Comput. Chem.* **1998**, *19*, 1639−1662.
(35) Huey, R.; Morris, G. M.; Olson, A. J.; Goodsell, D. S. *J. Comput. Chem.* **2007**, *28*, 1145−1152.
(36) DeLano, W. L. *The PyMOL molecular graphics system*; DeLano Scientific: San Carlos, USA, 2004http://pymol.sourceforge.net/ (accessed January 27, 2017).
(37) Case, T. A. D. D. A.; Cheatham, T. E.; Simmerling, C. L.; Wang, J.; Duke, R. E.; Luo, R.; Walker, R. C.; Zhang, W.; Merz, K. M.; Roberts, B.; Hayik, S.; Roitberg, A.; Seabra, G.; Swails, J.; Goetz, A. W.; Kolossvai, I.; Wong, K. F.; Paesani, F.; Vanicek, J.; Wolf, R. M.; Liu, J.; Wu, X.; Brozell, S. R.; Steinbrecher, T.; Gohlke, H.; Cai, Q.; Ye, X.; Wang, J.; Hsieh, M. J.; Cui, G.; Roe, D. R.; Mathews, D. H.; Seetin, M. G.; Salomon-Ferrer, R.; Sagui, C.; Babin, V.; Luchko, T.; Gusarov, S.; Kovalenko, A.; Kollman, P. A. *AMBER 12*; University of California: San Francisco, CA, 2012.
(38) Case, D. A.; Cheatham, T. E.; Darden, T.; Gohlke, H.; Luo, R.; Merz, K. M.; Onufriev, A., Jr.; Simmerling, C.; Wang, B.; Woods, R. J. *J. Comput. Chem.* **2005**, *26*, 1668−1688.
(39) Walker, R. C.; Crowley, M. F.; Case, D. A. *J. Comput. Chem.* **2008**, *29*, 1019−1031.
(40) Lindorff-Larsen, K.; Piana, S.; Palmo, K.; Maragakis, P.; Klepeis, J. L.; Dror, R. O.; Shaw, D. E. *Proteins: Struct., Funct., Genet.* **2010**, *78*, 1950−1958.
(41) Roe, D. R.; Cheatham, T. E. *J. Chem. Theory Comput.* **2013**, *9*, 3084−3095.
(42) Treesuwan, W.; Hannongbua, S. *J. Mol. Graphics Modell.* **2009**, *27*, 921−929.
(43) Zhou, Z.; Madura, J. D. *Proteins: Struct., Funct., Genet.* **2004**, *57*, 493−503.

DOI: 10.1021/acs.jnatprod.7b00155
J. Nat. Prod. XXXX, XXX, XXX−XXX